A Variable Stiffness Anthropomorphic Finger Through Embodied Intelligence Design

Julie Legrand, Huijiang Wang, Fumiya Iida, and Bram Vanderborght

Abstract—Most existing anthropomorphic robotic fingers are either too stiff to offer compliance, or too soft to provide postural stability. Yet human subjects tend to stiffen their finger when producing fingertip forces and lower their joint stiffness when grasping objects. Variable joint stiffness is therefore required to offer compliance and postural stability to the finger when interacting with its environment. We therefore propose the novel design of a robotic anthropomorphic finger capable of variable stiffness by making use of the embodied intelligence design principle through multifunctionality of the hardware parts. The ligaments of the finger are not only used to connect the phalanges together, but also to provide local variable stiffness at the finger joints through the use of miniature McKibben pneumatic artificial muscles. This novel design can therefore offer compliance at lower stiffness levels and postural stability and a higher applied force at higher stiffness levels while keeping the finger look and movement anthropomorphic and its control quite basic. The developed anthropomorphic finger with variable stiffness was tested by interacting with a flat surface. The finger presented a significantly higher stiffness ($6.7 \cdot 10^{-3} \pm 3 \cdot 10^{-3}$ Nm/rad) when the stiffening system was used than when the finger was purely used in compliance mode, without stiffness adaptation ($4.8 \cdot 10^{-3} \pm 0.7 \cdot 10^{-3}$ Nm/rad).

Index Terms—Biomimetics, Hydraulic/Pneumatic Actuators, Mechanism Design, Prosthetics and Exoskeletons.

I. INTRODUCTION

THE human hand is a complex biomechanical structure composed of interconnected bones, muscles, tendons, ligaments and nerves. This particular tissue layout allows the human to have about 20 degrees of freedom [1] and therefore perform complex grasping tasks.

The latest robotic reproductions of the anthropomorphic hand [2]–[4], although providing interesting solutions for anthropomorphic grasping, cannot actively adapt to different types of interactions the fingers experience with its environment. More specifically, those prototypes fall into two

categories: some are excessively rigid, which prevents them from deforming with the shape of objects and addressing the control instability issues associated with force feedback control at the tip. On the other hand, some are too soft to provide postural stability when the finger is pushing on a flat surface. Humans, however, are able to intentionally adjust the overall stiffness (or stiffness at the tip) of their fingers when exerting fingertip forces to enhance postural stability [5]. Postural stability refers to the fact that the finger can resist snapping into a hyperextended posture. Multilink mechanisms like our fingers are susceptible to buckle under tip forces. Suppressing this postural instability is crucial for hand dexterity [5]. Moreover, low finger joint stiffness is preferred at small flexion angles to allow proper dexterity in grasping objects with various sizes and shapes while high finger joint stiffness at larger flexion angles allows the finger to resist to out-of-plane deformations [6].

In order to mimic this change in finger overall stiffness according to the interaction the fingers experience with their environment, some prototypes have been proposed, such as the bionic hand of Zhang *et al.* and of Grebenstein *et al.*, offering overall variable stiffness through the antagonistic drive principle [7] using two truncated cone springs attached to rigid links [8] and tendons [9], respectively actuated by motors. The robotic fingers proposed by Luong *et al.* and Hino *et al.* use the same antagonistic drive principle as [7]–[9], where twisted-coiled polymer actuators (TCAs) [10] and shape memory alloy (SMA) wires [11] are respectively connected in series with a servomotor. Upon heat application, those TCA and SMA wires contract, which pull on the antagonistic connected tendons to create variable stiffness. The antagonistic drive principle, however, presents two main drawbacks. First, it requires a large force to be applied on the cable that is used to actuate the bending of the finger since it needs to counteract the forces applied on the antagonistic cables used for stiffening the finger. Second, the combined effect of the bending and stiffening cables actuation makes the control of the finger bending angle and overall stiffness complex. Note that, in this paper, the term *control* refers to a method of control theory. To limit the effect of the stiffening mechanism on the bending angle of the finger, Yan *et al.* proposed a robotic finger composed of conductive thermoplastic starch polymers (CTPSs) embodied in the finger phalanges [12]. Their stiffness can be independently adjusted by heating them up using thermistors or cooling them down using fluidic channels. The main limitation of this prototype is that the change in stiffness takes more than 10 seconds due to the slow cooling time of the CTPS, which prevent rapid stiffness adjustments.

In this work, we tackle the limitations of existing variable stiffness fingers by introducing a novel robotic anthropomorphic finger capable of variable joint stiffness by making use of the embodied intelligence design principle through multifunctionality of the hardware parts [13]. More specifically, the ligaments of the finger are not only used to connect the phalanges together, but also to provide local variable stiffness at the finger joints. This embodied intelligence design principle is called *static multifunctionality*: when a component is used to achieve more than one functionality by exploiting various intrinsic features [13]. The ligaments are made out of miniature McKibben pneumatic artificial muscles. Under pressurization, the artificial muscles contract and apply a normal force on the phalanges, which increases the joint stiffness. Regulating the input pressure of the ligaments therefore allows regulating the finger overall stiffness. By using this novel stiffening technique, which acts at the joint level, the control of the finger bending is simplified in comparison with the antagonistic drive principle. In fact, the variable stiffness system does not interfere with the bending actuation system. The presented design relies on the hypothesis that higher stiffness offers higher postural stability [5]. Therefore, the anthropomorphic finger offers compliance at lower stiffness levels, and postural stability while keeping a high applied force at higher stiffness levels.

II. DESIGN OF THE ANTHROPOMORPHIC FINGER

The finger is composed of 3D printed hollow phalanges linked to each other by miniature McKibben pneumatic artificial muscles, representing the ligaments (Figure 1). The phalanges design is based on the design of Hughes *et al.* [14]. The McKibben muscles are hand made using a braid made of Polyamide 6, coated with a thin layer of silicone (Ecoflex 00-30, Smooth-on, USA). Therefore, instead of using a balloon inside the braid [15], [16], the braid is integrated in the silicone layer. By using this manufacturing technique, a large range of McKibben muscle diameters and sizes can be made with a minimum diameter of 2 mm and a minimum length of 5 mm, which are fixed by manufacturing constraints. For the present anthropomorphic finger, the size of the McKibben muscles were chosen as small as possible to keep the prototype compact. Therefore, McKibben muscles of 2 mm diameter and 19.9±0.24 mm long were used to connect the phalanges together. To limit the amount of pressure supply tubes, the muscles are assembled in series at each side of the finger. The muscles are connected together using a 1 mm diameter silicone tube glued to the muscles using a silicone glue (Sil-Poxy, Smooth-on, USA). The muscles are then externally fixed to the phalanges using an epoxy glue (EA3430, Loctite, Henkel Adhesives, Germany) while their connected silicone tubes are placed inside the hollow phalanges (Figure 1). Both phalanges parts are then joined to each other using the same epoxy glue. For aesthetic purposes and to show the potential of the anthropomorphic finger of being integrated in a full anthropomorphic hand, we designed a full hand where the index is capable of variable joint stiffness and where the other fingers are passive. The hand is composed of a variable stiffness index and thumb. The palm is 3D printed in ABS, in which the fingers are fixed and glued using epoxy glue. To maintain the index in a given position (straight or bent), two antagonistic nylon cables are at one end attached to the finger tip, and at the other end to a 3D printed pulley fixed to a servo motor (Micro Servo 9g FS90, Feetech, China). The nylon wires are passed through metallic guides which are glued on the phalanges using an epoxy glue (Figure 2).

III. VARIABLE STIFFNESS PRINCIPLE AND MODEL

By actuating both McKibben muscles, representing the ligaments, the normal force between the phalanges will increase, which causes an increase of the normal and tangential contact stiffness at the joints. To model this phenomenon, we need to model the force applied by both McKibben muscles on the phalanges. To do so, we assume that the McKibben muscles are straight, parallel to the phalanges. The static modeling of the McKibben muscle described by Chou and Hannaford [17] can therefore be used. This model is based on the equivalence between the virtual work of the equilibrium force against the muscle contraction force and the virtual work of the pressure forces inside the balloon. The force F_N can therefore be expressed as a function of the input pressure P:
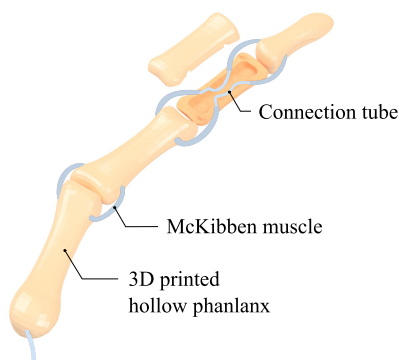

Fig. 1. Illustration of the finger assembly. The phalanges are 3D printed and hollow, linked together by miniature McKibben pneumatic artificial muscles, representing the ligaments. The McKibben muscles are connected together using silicone connection tubes.
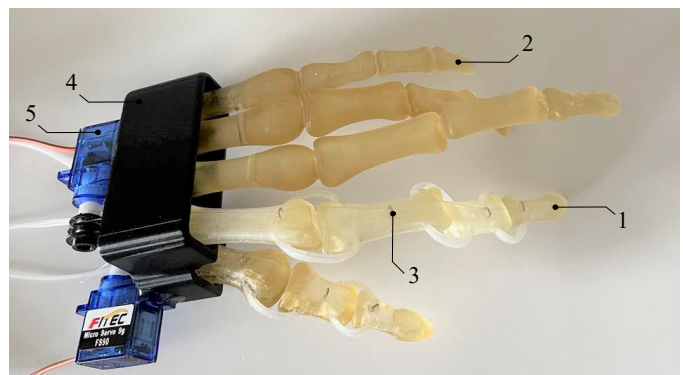

Fig. 2. Assembly of the full anthropomorphic hand with variable stiffness index and thumb. 1. Anthropomorphic finger with variable joint stiffness. 2. Aesthetic anthropomorphic finger without variable stiffness. 3. Nylon wire passing through metallic guides. 4. 3D printed palm. 5. Servo motor.

$$F_N(P) = \frac{Pb^2(2\cos^2(\theta) - \sin^2(\theta))}{4\pi n^2}, \quad (1)$$

where θ is the angle between a braided thread and the cylinder long axis, n, number of turns of a thread, and b, the thread length. Equation (1) can be rewritten as:

$$F_N(P) = \frac{\pi D_0^2 P}{4}(3\cos^2\theta - 1), \quad (2)$$

with $D_0 = b/n\pi$ being the diameter of the muscle when θ equals 90° [17].

Actuating the McKibben muscles at the joint level will increase the stiffness of the joint system through two phenomena. First, by increasing the normal force one phalanx applies on the other, and second, by increasing the bending stiffness of both McKibben muscle through pressurization.

Increasing the normal force between both phalanges will increase the joint stiffness against torques in the transversal plane (i.e. torques causing flexion or extension of the joint). To model this phenomenon, we apply an arbitrary torque M to the free phalanx (Figure 3), which causes the free phalanx to tilt with an angle α. When actuating the McKibben muscle, the latter produces a force F_N, according to (2). This normal force F_N will cause a friction moment defined as $M_f = r\mu F_N$, where r is the radius of the phalanx head, and μ is the friction coefficient between the fixed and the free phalanges (Figure 3). By using the energy conservation principle, one can write:

$$\alpha(M - M_f) = \frac{1}{2}I\omega^2, \quad (3)$$

where I is the moment of inertia of the free phalanx and ω is the angular velocity. The free phalanx can be approximated by a cylinder of length L_p. Therefore,

$$I = \frac{1}{3}mL_p^2. \quad (4)$$

This mass m can be expressed in function of the normal force F_N by using the dynamic McKibben contraction equation, which can be written as follows [18]:

$$m\ddot{x} = F_N - mg, \quad (5)$$

with m, the load driven by the muscle against gravity, and x, the muscle position. During constant velocity steady state, $\ddot{x} = 0$. Therefore,

$$F_N = mg. \quad (6)$$

By using (6) in (4) and (4) in (3), we obtain

$$\alpha(M - M_f) = \frac{F_N}{6g}L_p^2\omega^2. \quad (7)$$

By further expressing ω in function of α:

$$\alpha(M - M_f) = \frac{F_N}{6g}L_p^2\left(\frac{\alpha}{t}\right)^2. \quad (8)$$

By rearranging (8), we obtain:

$$M = \frac{F_N}{6g}L_p^2\frac{\alpha}{t^2} + M_f, \quad (9)$$

with t being the time it takes to move the phalanx form rest to an angle α when applying a torque M on the phalanx. The slope of (9) represents the joint stiffness in (Nm/rad). Therefore, the joint stiffness κ^t is written:

$$\kappa^t = \frac{F_N L_p^2}{6gt^2}. \quad (10)$$

From (8), we see that the joint stiffness is directly proportional to the force generated by the McKibben muscles.

To model the stiffness of the entire joint system, the bending stiffness of both McKibben muscles also need to be taken into account. The McKibben muscle is then seen as a tube with a material Young's modulus E, a length L_m, an outer diameter D_o, and an inter diameter D_i. The bending stiffness of one muscle is therefore calculated as:

$$\kappa^m = \frac{E\pi}{64L_m}(D_o^4 - D_i^4). \quad (11)$$

It is assumed that the muscle diameter increases linearly with the input pressure between D_{min} (the diameter at rest) and D_{max} (the diameter at maximum pressure). Therefore,

$$D_o = \frac{P}{P_{max}}(D_{max} - D_{min}) + D_{min} \quad (12)$$
$$D_i = D_o - 2t_m, \quad (13)$$

with t_m representing the muscle wall thickness. The total stiffness of the joint system is therefore expressed as:

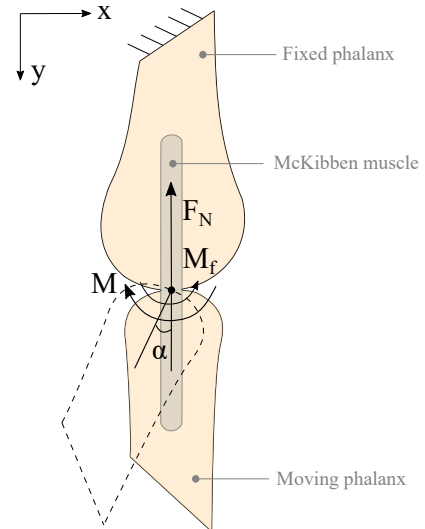$$\kappa = \kappa^t + \kappa^m. \quad (14)$$

Fig. 3. Forces and torques applied on a finger joint in the sagittal plane upon actuation of the McKibben muscles and application of an arbitrary torque M on the moving phalanx to calculate the joint stiffness.

IV. EXPERIMENTAL HAND CHARACTERIZATION

In this section, the different components of the anthropomorphic hand as well as their integration to the hand are tested. More specifically, the McKibben muscles used as ligaments are first separately characterized and their manufacturing disparity is quantified. Then, the integration of those muscles as ligaments in the anthropomorphic finger is tested and characterized. Finally, the stiffness model described in the previous section is experimentally verified by characterizing the stiffness of a finger joint.

A. McKibben muscle characterization

Since the McKibben muscles are hand made, those needs to be characterized. To do so, three McKibben muscles of 2.5 mm diameter and 25 mm long, without taking the attachment length into account, were made (Figure 4). To measure the force such a muscle can deliver, the muscles were repeatedly actuated by applying a three-cycle triangle pressure signal from 0 to 0.7 bar. The input pressure was set using a pressure regulator valve VEAB-L-26-D7-Q4-V1-1R1 (Festo, Esslingen am Neckar, Germany). To control the regulator valve, an Arduino with a PWM signal and a low-pass filter were used. The muscles were clamped to a frame at one end and to a 0.6 kg load cell (RS PRO Load Cell, RS, UK). The load cell data were read by the Arduino. Figure 5 depicts the results of those tests. The experimental force the McKibben could deliver was compared to the theoretical model (Figure 5), i.e. to eq. (2), with $b = 35$ mm, $\theta = 0.44$ rad and $n = 5$. Those values were manually measured on the manufactured McKibben muscles.

As seen in Figure 5, the experimental force does not vary linearly in function of the input pressure. A plausible explanation for this is the fact that the silicone layer was manually applied on the braid. It is then possible that the braid is not everywhere perfectly integrated into that silicone layer. This would limit the muscle contraction. One can also notice that the muscles present manufacturing inaccuracies since three identically made muscles present different output force curves. The maximum force disparity was measured at 0.7 bar and equals 0.65 N.
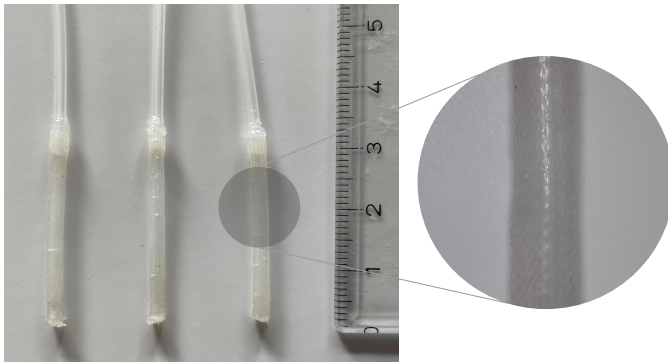

Fig. 4. Three handmade McKibben muscles of 2.5 mm diameter and 25 mm long used for the characterization of the artificial muscle ligaments of the anthropomorphic finger.
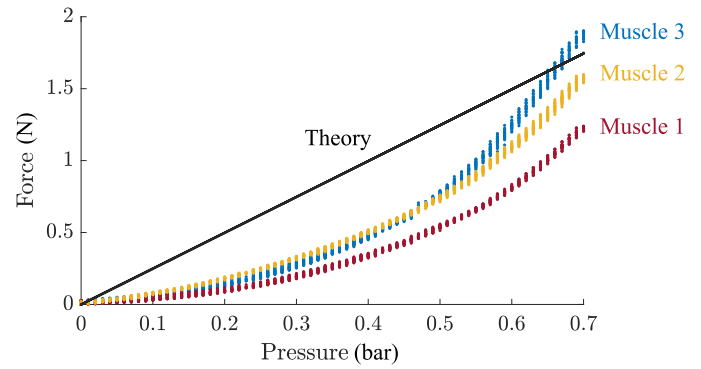

Fig. 5. Comparison between the theoretical and the experimental force generated by three handmade McKibben muscles upon the application of a three-cycle triangle pressure signal from 0 to 0.7 bar.
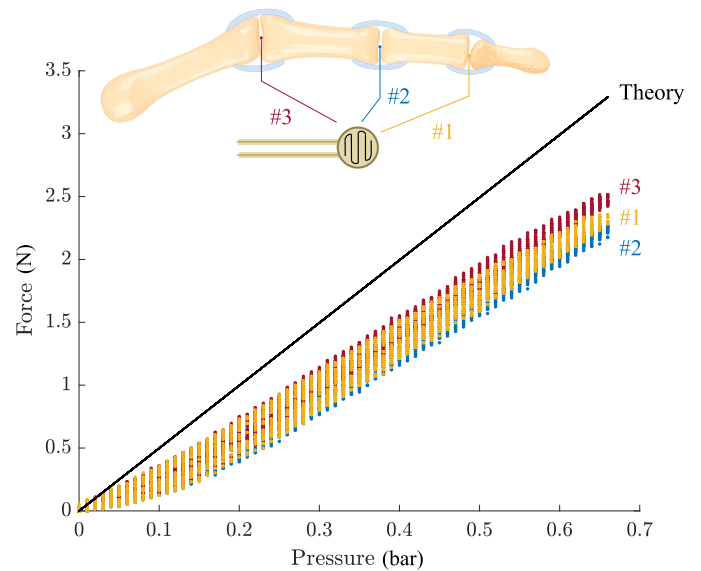

Fig. 6. Force measured between each phalanx upon actuation of the McKibben muscle of the anthropomorphic finger by applying a seven-cycle triangle pressure signal from 0 to 0.7 bar and comparison to the theoretical values.

B. McKibben muscle implementation

The McKibben muscles were attached to the phalanges according to the manufacturing technique described in Section II to form the anthropomorphic finger with variable stiffness capabilities through actuation of the ligaments. The normal force F_N was measured at each joint by placing a thin pressure sensor (Joy-it pressure sensor 10 kg, Simac Electronics, Germany) along the transverse plan of the finger, between the phalanges. The McKibben muscle ligaments were actuated using a seven-cycle triangle pressure signal from 0 to 0.7 bar. The measured normal force F_N at each joint is reported in Figure 6, as well as the theoretical force value, which is $2F_N$ for each joint. As visible in Figure 6, the experimental normal force is lower than the theoretical one with an average of 0.95 N at 0.7 bar. This is due to the fact that the McKibben muscles are not straight anymore, once integrated into the anthropomorphic finger, but form a semicircle around the joint. A portion of the muscle ends is pressed against the phalanx
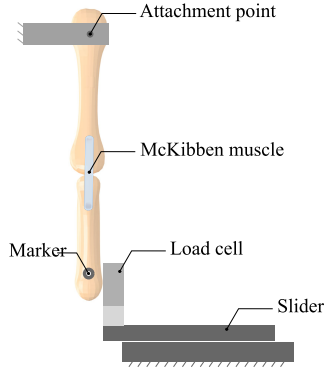
Fig. 7. Set-up used to evaluate the joint stiffness of the anthropomorphic finger.

TABLE I
STIFFNESS MODEL PARAMETERS

Parameter	Value	Parameter	Value
E	0.7 GPa	b	35 mm
L_m	22.5 mm	n	5
D_{min}	2.5 mm	θ	0.44 rad
D_{max}	2.7 mm	L_p	35 mm
t_m	0.7 mm	t	0.016 s

which causes that part to not inflate properly and therefore limits the ability of the muscle to deliver its maximum force.

C. Joint stiffness characterization

To evaluate the joint stiffness of the anthropomorphic finger, the set-up depicted in Figure 7 was used. One of the phalanges was fixed to the frame, while the other was let free. To measure the force applied on the tip of the free phalanx, a 0.6 kg load cell (RS PRO Load Cell, RS, UK) was used, clamped to a slider. The slider was manually actuated using a screw to push against the free phalanx tip. To measure the displacement, a marker was placed at the free phalanx tip and its position was recorded with a camera. To obtain the stiffness, the slope of the force in function of the displacement graph was calculated. This was done for different values of input pressure set in the McKibben muscles. Figure 8 depicts the results of those tests and compare them to the theoretical values obtained using the equation (14) and the parameter values reported in Table I.

The Young modulus of the McKibben muscle material E was fixed by considering that 75% of the muscle is made out of silicone (Ecoflex 00-30, Smooth-on, USA), which has a Young modulus of 0.125 MPa [19], and the 25 % resting, made of Polyamide 6, which has a Young modulus of 2.8

GPa [20]. The muscle length L_m, the smallest and largest muscle diameters D_{min} and D_{max}, the muscle wall thickness t_m and the length of the free phalanx L_p were all manually measured. The muscle parameters b and n were measured on a handmade muscle, and θ was precisely measured using a microscope. The time constant t was found by minimizing the root mean square error (RMSE) of the theoretical curve with respect to the experimental data. As a result, an RMSE of 4.6% was calculated between the theoretical curve and the experimental points, which validates the theoretical model described in Section III.

V. INTERACTION WITH A FLAT SURFACE

The index of the anthropomorphic hand was slightly bent using the servo motor to tension the tendons and placed on the tip of a 0.6 kg load cell (RS PRO Load Cell, RS, UK). The hand was then manually moved downwards to exert some force on the load cell. Ten pushing movements were conducted on the load cell while the load cell data and the scene (using a camera) were recorded. This test was repeated twice. Once with the activation of the variable stiffness system, i.e. by pressurizing the McKibben muscle, and once without. The pressure in the McKibben muscle was set proportional to the pushing force measured by the load cell. This choice of set pressure was made following what can be observed in nature, i.e. that humans appear to make the limb stiffer when applying larger forces on a surface [5].

The pressure reaches a maximum of 0.65 bar when the measured force reaches 0.17 N. The finger stiffness was calculated at maximum recorded force during each pushing movement on the load cell. As a result of those 20 tests (10 pushing movements with McKibben muscle activation and 10 without), the finger stiffness was evaluated to be $6.7 \cdot 10^{-3} \pm 3 \cdot 10^{-3}$ Nm/rad when the stiffening system was activated and $4.8 \cdot 10^{-3} \pm 0.7 \cdot 10^{-3}$ Nm/rad when it was not. The large standard deviation for the measurements with stiffening system activated is explained by the fact that this system actively changes its stiffness in real time in function of the sensed force. Any delay in the stiffness regulation can therefore cause discrepancies in the data.

To check if this difference is significant, a Wilcoxon signed-rank test was applied to both data samples. The Wilcoxon signed-rank test was chosen here because of the limited size of the data samples, which does not ensure that the data follows a normal distribution. As a result, the null hypothesis was rejected with a significance level of 5%, which indicates that
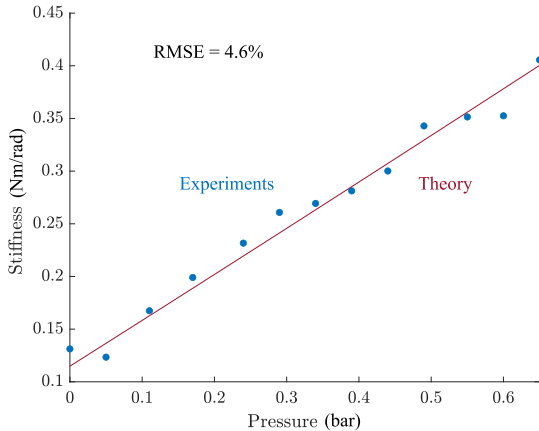

Fig. 8. Experimental values compared to the theory (eq. (14)) of the joint stiffness of the anthropomorphic finger in function of the pressure applied to the McKibben muscle ligaments.
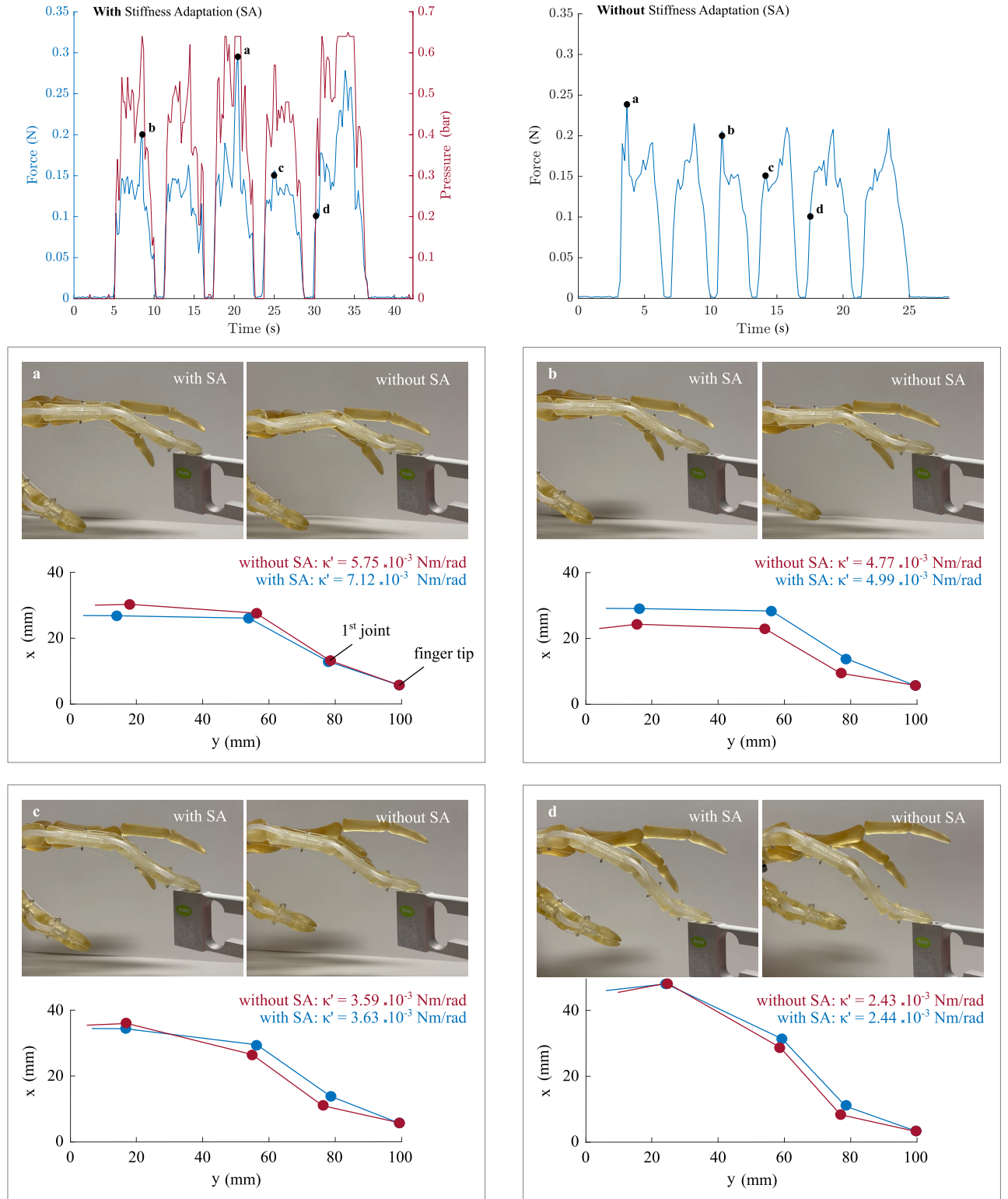
Fig. 9. Anthropomorphic index pushing on a flat surface. The index tip is placed on a load cell and repeatedly moved downwards to exert some force on it. The test is first performed with stiffness adaptation, i.e. with activation of the McKibben muscles, (top left), then without stiffness adaptation (top right). At 0.2, 0.15, 0.1 N and at maximal force, the joint positions are plotted, represented by the dots, and the stiffness κ' is calculated.

the variable stiffness system of the anthropomorphic finger is capable of providing a significantly higher stiffness than when used in compliant mode (i.e. when the stiffening system is not used). As an illustration of this test, 5 pushing movements are reported in Figure 9. The full data point set is reported in the top of Figure 9. On this test, four different points were analyzed (a,b,c and d). Point a represents the point with the maximum force measured. Points b, c and d are the points

taken at 0.05 N intervals to illustrate the stiffening effect on a decreasing applied force. The maximum force measured when the stiffness system is on is 0.29 N, while a maximum force of 0.24 N was measured when the system is off. The effect of the stiffness activation can be seen in Figure 9 at the measured point a. At that point, the pressure applied to the McKibben muscles is maximum (0.65 bar), which results in a finger overall stiffness of $7.12 \cdot 10^{-3}$ Nm/rad, compared to a stiffness of $5.75 \cdot 10^{-3}$ Nm/rad when the stiffness system is not activated. To calculate the deformation, and therefore calculate this stiffness, the angle between two consecutive phalanges was measured at each joint, and the mean was taken as a measure of the finger deformation. In Figure 9a, one can notice the visual difference between an index push with and without stiffness activation. The finger undergoes a larger deformation when the stiffness system is not activated. At 0.2 N, the pressure applied to the McKibben muscles is also set at its maximum (0.65 bar) and an overall stiffness of $4.99 \cdot 10^{-3}$ Nm/rad is calculated, compared to $4.77 \cdot 10^{-3}$ Nm/rad when the stiffness system is off. Again, one can notice a larger deformation of the finger when no pressure is applied to the McKibben muscles (Figure 9b). At 0.15 and 0.1 N, the measured overall stiffness becomes more similar whether the system is on or off. This is because the applied pressure was set decreasing with the applied force. At 0.15 N, the pressure is set at 0.57 bar while at 0.1 N, the pressure is set at 0.2 bar.

Using higher pressure in the McKibben muscles, and therefore increasing the finger overall stiffness allows applying force on a flat surface while keeping proper postural stability. Decreasing the pressure and therefore reducing the finger overall stiffness allows providing a more compliant push on the surface, which can be more appropriate to interactions with delicate and fragile objects.

VI. DISCUSSION

The anthropomorphic finger prototype presented in this paper is a first attempt towards the creation of compliant and stable interactions while relying on the finger anatomical components only to switch between compliance and higher stiffness, which leads to high applied forces while keeping postural stability [5].

This first prototype presented in this paper would need more connective tissues to really mimic anthropomorphic movements, such as extra ligaments, tendons and skin. However, the purpose of the present study is to demonstrate the potential of the variable stiffness system consisting of using miniature McKibben muscle as ligaments to locally change the joint stiffness. Although an increase in overall stiffness is recorded when activating the variable stiffness system, this increase could even reach higher levels by using bigger McKibben muscles as ligaments. Of course a trade-off is then necessary between larger McKibben muscles (and therefore larger applied force and stiffness) and anthropomorphism.

It is also important to note the following limitation of the presented variable stiffness system. The McKibben muscles always need to be activated when the finger is at its target position. If the McKibben muscles are activated while the finger is in movement (by pulling on the tendons), this could cause excessive friction at the finger joints and therefore have a negative impact on the proper control of the finger movements.

The presented variable stiffness system cannot only be used in the field of hand prostheses and exoskeletons, but also in the field of minimally invasive surgical robotics. One of the main challenges in endoscopic surgery nowadays is the lack of variable stiffness of the instrument used. Endoscopes need flexibility to reach the pathology through the tortuous paths that are human lumina while being rigid to grasp and manipulate tissues with their tips [21]. The variable stiffness system presented in this paper can therefore be a solution for discrete links endoscopes, which can be comparable to the phalanges of the anthropomorphic finger. For endoscopic applications, the McKibben muscle making the links between the discrete links could also be actuated separately, by connecting them with different tubes attached to different pressure valves. This would allow regulating the stiffness at different places along the endoscope, which can be beneficial for some surgical procedures [21].

VII. CONCLUSION

In this work, a new robotic anthropomorphic finger capable of variable stiffness is presented that makes use of the embodied intelligence design principle through multifunctionality of the hardware parts. The ligaments of the finger are not only used as connecting tissue, but they also provide local variable stiffness at the finger joints. The ligaments are made out of miniature McKibben pneumatic artificial muscles which contract under pressure and apply a normal force on the phalanges, increasing the joint stiffness. By regulating the pressure inside the McKibben muscle, different levels of stiffness can be achieved. Compliance is offered at lower stiffness levels while higher stiffness levels provide high applied force coupled with postural stability. This variable stiffness system design offers a solution to the limitations of fingers using the antagonistic drive principle, i.e. their complex control due to the combined effect of the bending and stiffening cable actuation. Indeed, the developed anthropomorphic finger can bend using tendons and once at a desired position, be stiffened by pressurizing the McKibben muscles. The variable stiffness system does not interfere with the bending actuation system. The finger stiffness was significantly higher ($6.7 \cdot 10^{-3} \pm 3 \cdot 10^{-3}$ Nm/rad) when the stiffening system was activated than when it was not ($4.8 \cdot 10^{-3} \pm 0.7 \cdot 10^{-3}$ Nm/rad). Future work will consist in exploiting this variable stiffness system further to perform more complex compliant and stable interactions by e.g. let the anthropomorphic hand with variable stiffness execute the tip pinch and palmar grasp.

REFERENCES

[1] V. K. Nanayakkara, G. Cotugno, N. Vitzilaios, D. Venetsanos, T. Nanayakkara, and M. N. Sahinkaya, "The role of morphology of the thumb in anthropomorphic grasping: a review," *Frontiers in mechanical engineering*, vol. 3, p. 5, 2017.

[2] C. Zhang, M. Li, Y. Chen, Z. Yang, B. He, X. Li, J. Xie, and G. Xu, "An anthropomorphic robotic hand with a soft-rigid hybrid structure and positive-negative pneumatic actuation," *IEEE Robotics and Automation Letters*, 2023.

[3] H. Zhou, C. Tawk, and G. Alici, "A 3d printed soft robotic hand with embedded soft sensors for direct transition between hand gestures and improved grasping quality and diversity," *IEEE Transactions on Neural Systems and Rehabilitation Engineering*, vol. 30, pp. 550–558, 2022.

[4] A. K. Sinha, N. M. Thalmann, and Y. Cai, "Measuring anthropomorphism of a new humanoid hand-arm system," *International Journal of Social Robotics*, pp. 1–23, 2023.

[5] N. Sharma and M. Venkadesan, "Finger stability in precision grips," *Proceedings of the National Academy of Sciences*, vol. 119, no. 12, p. e2122903119, 2022.

[6] Y. Zhu, G. Wei, L. Ren, Z. Luo, and J. Shang, "An anthropomorphic robotic finger with innate human-finger-like biomechanical advantages part i: Design, ligamentous joint, and extensor mechanism," *IEEE Transactions on Robotics*, 2022.

[7] W. Friedl, H. Höppner, F. Petit, and G. Hirzinger, "Wrist and forearm rotation of the dlr hand arm system: Mechanical design, shape analysis and experimental validation," in *2011 IEEE/RSJ International Conference on Intelligent Robots and Systems*. IEEE, 2011, pp. 1836–1842.

[8] X. Zang, C. Wang, P. Zhang, G. Liu, X. Zhang, and J. Zhao, "A novel design of a multi-fingered bionic hand with variable stiffness for robotic grasp," *Journal of Mechanisms and Robotics*, vol. 15, no. 4, p. 045001, 2023.

[9] M. Grebenstein, M. Chalon, G. Hirzinger, and R. Siegwart, "Antagonistically driven finger design for the anthropomorphic dlr hand arm system," in *2010 10th IEEE-RAS International Conference on Humanoid Robots*. IEEE, 2010, pp. 609–616.

[10] T. Luong, S. Seo, J. Hudoklin, J. C. Koo, H. R. Choi, and H. Moon, "Variable stiffness robotic hand driven by twisted-coiled polymer actuators," *IEEE Robotics and Automation Letters*, vol. 7, no. 2, pp. 3178–3185, 2022.

[11] T. Hino and T. Maeno, "Development of a miniature robot finger with a variable stiffness mechanism using shape memory alloy," *Proceedings of The International Simposium on Robotics and Automation*, pp. 214–218, 2004.

[12] J. Yan, Z. Xu, P. Shi, and J. Zhao, "A human-inspired soft finger with dual-mode morphing enabled by variable stiffness mechanism," *Soft Robotics*, vol. 9, no. 2, pp. 399–411, 2022.

[13] M. Cianchetti, "Embodied intelligence in soft robotics through hardware multifunctionality," *Frontiers in Robotics and AI*, vol. 8, p. 724056, 2021.

[14] J. Hughes, P. Maiolino, and F. Iida, "An anthropomorphic soft skeleton hand exploiting conditional models for piano playing," *Science Robotics*, vol. 3, no. 25, p. eaau3098, 2018.

[15] J. Legrand, B. Loenders, A. Vos, L. Schoevaerdts, and E. Vander Poorten, "Integrated capacitance sensing for miniature artificial muscle actuators," *IEEE Sensors Journal*, vol. 20, no. 3, pp. 1363–1372, 2019.

[16] J. Legrand, M. Ourak, and E. B. Vander Poorten, "Concentric muscles–miniature pneumatic actuator with integrated channel for surgical instruments," in *ACTUATOR; International Conference and Exhibition on New Actuator Systems and Applications 2021*. VDE, 2021, pp. 1–4.

[17] C.-P. Chou and B. Hannaford, "Measurement and modeling of mckibben pneumatic artificial muscles," *IEEE Transactions on robotics and automation*, vol. 12, no. 1, pp. 90–102, 1996.

[18] B. Tondu, "Modelling of the mckibben artificial muscle: A review," *Journal of Intelligent Material Systems and Structures*, vol. 23, no. 3, pp. 225–253, 2012.

[19] J. Shintake, H. Sonar, E. Piskarev, J. Paik, and D. Floreano, "Soft pneumatic gelatin actuator for edible robotics," in *2017 IEEE/RSJ International Conference on Intelligent Robots and Systems (IROS)*. IEEE, 2017, pp. 6221–6226.

[20] J. Huang, W. Ulrich, S. Schmauder, and S. Geier, "Micro-mechanical modelling of young's modulus of semi-crystalline polyamide 6 (pa 6) and elastomer particle-modified-pa 6," *Computational materials science*, vol. 50, no. 4, pp. 1315–1319, 2011.

[21] M. W. Gifari, H. Naghibi, S. Stramigioli, and M. Abayazid, "A review on recent advances in soft surgical robots for endoscopic applications," *The International Journal of Medical Robotics and Computer Assisted Surgery*, vol. 15, no. 5, p. e2010, 2019.